ACS APPLIED MATERIALS & INTERFACES

Research Article

www.acsami.org

Symmetry Breaking in Side Chains Leading to Mixed Orientations and Improved Charge Transport in Isoindigo-*alt*-Bithiophene Based Polymer Thin Films

Guobiao Xue,[†,‡,▽] Xikang Zhao,[†,▽] Ge Qu,[§] Tianbai Xu,[†,∥] Aristide Gumyusenge,[†] Zhuorui Zhang,[†,⊥] Yan Zhao,[†] Ying Diao,[§] Hanying Li,[*,‡] and Jianguo Mei[*,†,#]

[†]Department of Chemistry, Purdue University, West Lafayette, Indiana 47907, United States

[‡]MOE Key Laboratory of Macromolecule Synthesis and Functionalization, State Key Laboratory of Silicon Materials, Department of Polymer Science and Engineering, Zhejiang University, Hangzhou 310027, P. R. China

[§]Department of Chemical & Biomolecular Engineering, University of Illinois at Urbana—Champaign, 600 South Mathews Avenue, Urbana, Illinois 61801, United States

[∥]College of Information Science & Electronic Engineering, Zhejiang University, Hangzhou 310027, P. R. China

[⊥]Department of Chemistry, Tsinghua University, Beijing 100084, P. R. China

[#]Birck Nanotechnology Center, Purdue University, 1205 West State Street, West Lafayette, Indiana 47906, United States

Supporting Information

ABSTRACT: The selection of side chains is important in design of conjugated polymers. It not only affects their intrinsic physical properties, but also has an impact on thin film morphologies. Recent reports suggested that a face-on/edge-on bimodal orientation observed in polymer thin films may be responsible for a three-dimensional (3D) charge transport and leads to dramatically improved mobility in donor−acceptor based conjugated polymers. To achieve a bimodal orientation in thin films has been seldom explored from the aspect of molecular design. Here, we demonstrate a design strategy involving the use of asymmetric side chains that enables an isoindigo-based polymer to adopt a distinct bimodal orientation, confirmed by the grazing incidence X-ray diffraction. As a result, the polymer presents an average high mobility of 3.8 ± 0.7 $cm^2\ V^{-1}\ s^{-1}$ with a maximum value of 5.1 $cm^2\ V^{-1}\ s^{-1}$, in comparison with 0.47 and 0.51 $cm^2\ V^{-1}\ s^{-1}$ obtained from the two reference polymers. This study exemplifies a new strategy to develop the next generation polymers through understanding the property-structure relationship.

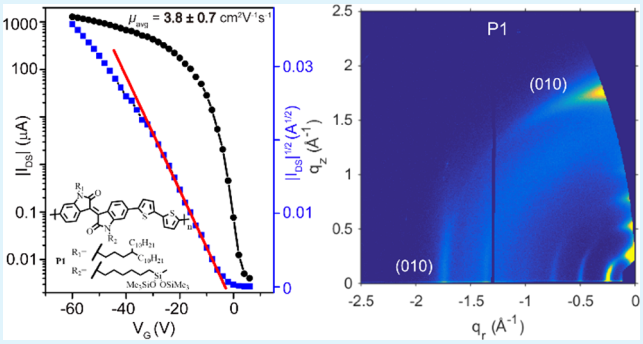

KEYWORDS: *asymmetric side chains, isoindigo-based polymers, field-effect transistors, bimodal orientation, three-dimensional charge transport*

INTRODUCTION

Semiconducting polymers present their unique potentials in low-cost, large-area, flexible, and printed optoelectronic devices.[1−5] Understanding charge transport and achieving high charge carrier mobilities are key to the realization of these potentials, yet challenging. Charge transport in polymer films is complicated. It is not only related to polymer chemical structures, but also the morphologies of the polymer thin films such as the molecular packing motifs, orientations and connectivities of polymer chains. In a conventional model, a two-dimensional (2D) charge transport takes place at the semiconductor/dielectric interface parallel to the substrate between source and drain electrodes.[6−9] Similar to the small molecules, an edge-on orientation with an in-plane $\pi-\pi$ stacking, in order for a significant current to be generated within the channel, is shown to favor charge transport.[10−13] On the contrary, a face-on orientation is usually not desired for an efficient charge transport in a transistor device. The study of highly crystalline polymers such as poly(3-hexylthiophene) (P3HT) and poly[2,5-bis(3-alkylthiophen-2-yl)thieno[3,2-*b*]-thiophene] (PBTTT) supports such a 2D charge transport model.[14] Recent studies on some donor−acceptor (D−A) polymers, however, have presented a different fact that the D−A polymer films containing mixtures of both edge-on and face-on orientations (bimodal orientation) at the interface could also offer highly efficient charge transport.[15−20] For instance, Zhang et al. described a series of highly soluble diketopyrrolopyrrole (DPP)−bithiophene copolymers with a variable

Received: May 29, 2017
Accepted: July 13, 2017
Published: July 13, 2017

DOI: 10.1021/acsami.7b07624
ACS Appl. Mater. Interfaces 2017, 9, 25426−25433

moiety of thienothiophene (TT), bithiophene (2T), or monothiophene (T) and found that the DPP-T polymer films with a bimodal orientation exhibited a surprisingly high mobility.[18]

The observation of a bimodal orientation and the associated efficient charge transport sparkle the interest of the three-dimensional (3D) charge transport model.[21−24] Demeyu et al. reported that charge carriers are confined in a conducting channel in the organic semiconductor with a thickness of about 5−6 nm.[21] Shehu et al. proved that the current starts to flow when percolation of the first monolayer occurs and, depending on the deposition rate, saturates at a coverage in the range of 2−7 monolayers.[24] Sharma et al. first proposed charge transport in organic field-effect transistors (OFETs) is essentially a 3D process.[22] Bao et al. introduced siloxane-terminated solubilizing groups as the side chain in an isoindigo-based polymer, which led to a smaller $\pi-\pi$ stacking distance in comparison with a reference polymer with a branched alkyl side chain. The polymer also showed a bimodal feature. They speculated that these two factors are the origins for the achieved high mobility of 2.48 $cm^2\ V^{-1}\ s^{-1}$.[15] Park et al. further confirmed that the bimodal orientation is more beneficial for 3D charge transport than a unimodal orientation by probing the temperature-dependent (80−350 K) charge transport with the same isoindigo-based polymer.[23] They concluded that polymer films with mixtures of edge-on and face-on orientations are highly desired for charge transport, provided that sufficient π-stacking remains at a molecular scale. Lee et al. reported a DPP−selenophene copolymer with mixed bimodal orientations exhibiting the best ambipolar transport (hole mobility of 8.84 $cm^2\ V^{-1}\ s^{-1}$ and electron of 4.34 $cm^2\ V^{-1}\ s^{-1}$).[16] Kim et al. achieved highly efficient electron transport in naphthalene diimide-based polymers with tuning the ratio of face-on and edge-on orientations through the selection of proper solvents. It was observed that the best performing films even have a less densely packed organization. These studies repeatedly suggested that a bimodal orientation can be a critical factor that governs charge transport.[17]

From the aspect of polymer design, however, it is less known how we can purposely enhance a bimodal orientation in a polymer thin film. A very recent effort is that Yang et al., studied the control of bimodal orientation via backbone engineering.[17] They reported two naphthalene diimide-based polymers that have identical side chains, but different conjugated backbones. P(NDI2SiC6-T2) consists of NDI and bithiophene (T2) repeating units, while for P(NDI2SiC6-TVT), the (*E*)-2-(2-(thiophen-2-yl)-vinyl)thiophene (TVT) units. The thin films from chloroform solutions would give a mixed bimodal orientation for P(NDI2SiC6-T2) and a preferential edge-on orientation for P(NDI2SiC6-TVT). Side chain engineering has emerged as a powerful tool to control charge transport properties.[25] In this work, we renew the concept of side chain engineering and introduce asymmetric side chains as solubilizing groups onto a conjugated backbone. Specifically, we designed a set of three polymers, P1, Ref-1 and Ref-2, which are all composed of isoindigo-bithiophene repeating units, to investigate how the side chains affect the polymer chain orientations and how they correlate with charge transport properties. P1 has a symmetry-breaking in its two side chains. One is an alkyl chain and the other is a siloxane hybrid chain. The two reference polymers (Ref-1[15] and Ref-2[26]) with symmetric side chains have been reported in literatures and set a ground for a fair comparison. Ref-1 has two identical siloxane hybrid chains, while Ref-2 has two identical alkyl chains. The chemical structures are shown in Scheme 1. We found that P1

Scheme 1. Synthetic Route for the Three Polymers

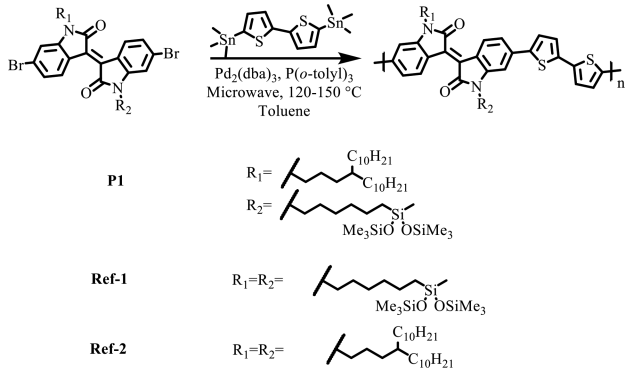

indeed has an enhanced bimodal orientation in thin films, confirmed by the study of grazing incidence X-ray diffraction (GIXRD) pattern. We also satisfyingly reported that P1 significantly outperforms the two reference polymers and exhibits an average mobility of 3.8 ± 0.7 $cm^2\ V^{-1}\ s^{-1}$ based on 20 tested devices, with the highest value of 5.1 $cm^2\ V^{-1}\ s^{-1}$. In addition, the mechanical studies revealed that P1 presents the lowest tensile modulus among the three polymers investigated both from bucking method (0.151 GPa) and nanoindentation measurement (0.179 ± 0.022 GPa), illustrating a high elasticity and flexibility.

EXPERIMENTAL SECTION

Materials and Characterizations. All reagents were purchased from Sigma-Aldrich and used without further purification unless otherwise noticed. 11-(3-Iodopropyl)henicosane was purchased from Lyntech and used without further purification. 6,6′-Bromoisoindigo,[27] Ref-1 and Ref-2[26] were synthesized based on methods previously reported. ^1H and ^{13}C NMR spectra were recorded using Varian Inova 300 and Bruker ARX 400 at 293 K with deuterated chloroform as solvent. Gel permeation chromatography (GPC) was performed in trichlorobenzene at 150 °C with a PL-GPC220 System. The results were obtained based on the calibration generated from polystyrene standards. UV−vis−NIR spectra were recorded on an Agilent Technologies Cary 6000i UV−vis−NIR spectrophotometer (300−1300 nm). Thermal gravimetric analysis (TGA) was performed with a TA Instruments Q50. The polymer sample was heated in a platinum cell from 40 to 800 °C at a rate of 10 °C/min with the furnace (60 mL/min) and balance (40 mL/min) purged with nitrogen. Differential scanning calorimetry (DSC) thermogram was measured using a TA Q5000 calorimeter. The polymer was sealed in a hermetic aluminum pan and measurd under nitrogen purge (50 mL/min). The sample was heated and cooled in two cycles between 0 to 300 °C, with the first cycle removing any thermal history of the sample. The heating and cooling rates for all measurements were 10 °C/min.

Synthesis of 6,6′-Dibromo-1-(4-decyltetradecyl)-1′-(hex-5-en-1-yl)isoindigo. To an oven-dried round-bottom flask with a magnetic stir bar was charged anhydrous *N*,*N*-dimethylformamide (20 mL), 6,6′-dibromoisoindigo (1.0 g, 2.4 mmol), 18-crown-6 (31 mg, 0.12 mmol), and potassium carbonate (2.0 g, 14 mmol). The mixture was heated at 100 °C for 1 h before a mixture of 11-(3-iodopropyl)henicosane (1.2 g, 2.6 mmol) and 6-iodo-1-hexene (0.55 g, 2.6 mmol) was added dropwise through a syringe. The mixture was kept at this temperature overnight. After being cooled to room temperature, water (50 mL) was added, and the mixture was extracted with hexanes (3 × 50 mL). The organic layers were combined, dried over magnesium sulfate and filtered. Solvents were removed in vacuo, and the product was purified via column chromatography with

DOI: 10.1021/acsami.7b07624
ACS Appl. Mater. Interfaces 2017, 9, 25426−25433

hexanes-dichloromethane (10:1 to 1:1) as the eluent. The product was obtained via precipitation from methanol (0.21 g, 21%). ^{1}H NMR (400 MHz, $CDCl_3$) δ 9.04 (d, J = 8.6 Hz, 2H), 7.13 (d, J = 8.6 Hz, 2H), 6.87 (s, 2H), 5.78 (m, 1H), 5.00 (m, 2H), 3.68 (m, 4H), 2.12 (m, 2H), 1.64 (m, 4H), 1.48 (m, 4H), 1.24 (m, 37H), 0.87 (t, J = 7.4 Hz, 6H). ^{13}C NMR (100 MHz, $CDCl_3$) δ 167.50, 167.47, 145.61, 145.50, 137.95, 132.44, 132.30, 131.12, 126.63, 126.61, 124.97, 120.25, 115.04, 111.09, 40.47, 39.89, 36.99, 33.42, 33.17, 31.83, 31.49, 30.69, 30.00, 29.60, 29.55, 29.26, 26.63, 26.57, 26.04, 24.35, 22.59, 14.03. MS (ESI, M + H$^+$) for $C_{46}H_{67}Br_2N_2O_2$: calcd. 837.3564 found 837.3578.

Synthesis of 6,6′-Dibromo-1-(4-decyltetradecyl)-1′-(6-(1,1,1,3,5,5,5-heptamethyltrisiloxan-3-yl)hexyl)isoindigo. 190 mg of 6,6′-dibromo-1-(4- decyltetradecyl)-1′-(hex-5-en-1-yl)isoindigo was dissolved in 10 mL of toluene. The solution was purged with nitrogen for 15 min. 74 μL of 1,1,1,3,5,5,5- heptamethyltrisiloxane and one drop of Karstedt's catalyst (2% in xylene, low color) was injected into the solution. The solution was heated at 50 °C and the reaction was monitored with TLC. The product was purified using flash column chromatography with hexanes−dichloromethane (3:2) as the eluent (72.6 mg, 30.2%). ^{1}H NMR (300 MHz, $CDCl_3$) δ 9.08 (dd, J_1 = 8.6 Hz, J_2 = 1.1 Hz, 2H), 7.17 (dd, J_1 = 8.6 Hz, J_2 = 1.8 Hz, 2H), 6.93 (d, J = 1.9 Hz, 2H), 3.72 (m, 4H), 1.67 (m, 4H), 1.40−1.12 (m, 45H), 0.87 (t, J = 6.3 Hz, 6H), 0.45 (t, J = 7.8 Hz, 2H), 0.08 (s, 18H), −0.01 (s, 3H). ^{13}C NMR (100 MHz, $CDCl_3$) δ 167.62, 145.68, 132.54, 131.11, 126.63, 125.03, 120.33, 111.20, 40.52, 40.20, 37.00, 33.42, 32.74, 31.82, 30.71, 29.99, 29.58, 29.25, 27.27, 26.57, 24.37, 22.90, 22.59, 17.46, 14.02, 1.77, −0.40. MS (ESI, M + H$^+$) for $C_{53}H_{89}Br_2N_2O_4Si_3$: calcd. 1059.4491 found 1059.4471.

Synthesis of P1. 5,5′-Bis(trimethylstannyl)-2,2′-bithiophene (33.5 mg, 68.0 μmol) and 6,6′-dibromo-1-(4-decyltetradecyl)-1′-(6-(1,1,1,3,5,5,5-heptamethyltrisiloxan-3-yl)hexyl)isoindigo (72.2 mg, 68.0 μmol) were charged in a 35 mL microwave vessel. The monomers were dissolved in 12 mL of anhydrous toluene and the solution was degassed with nitrogen for 15 min. $Pd_2(dba)_3$ (2.5 mol %) and tris(*o*-tolyl)phosphine (4 mol %) were quickly added to the solution under nitrogen. Sealed with a snap cap, the vessel was transferred to a CEM Discover Automatic Microwave Reactor. Reaction conditions: power cycling mode; power, 300 W; power cycles, 100; temperature, 120−150 °C; heating, 120s; cooling, 30s; pressure, 150 psi; and stirring, high. When the polymerization was complete, the mixture was precipitated into methanol, and the solids were collected by a high quality glass fiber thimble. The polymer was purified by Soxhlet extractions with acetone, hexane, and chloroform. The chloroform fraction was concentrated and palladium was removed with the addition of 15 mg of *N*,*N*-diethylphenylazothioformamide at 50 °C for 30 min. The product was collected from methanol and dried at 60 °C under high vacuum (42 mg, 56.3%).

Thin Film Preparation and Characteristics. The isoindigo-based polymer thin layer was deposited on the octadecyltrichlorosilane (OTS)-modified highly doped silicon substrates (with Au bottom contact) with 300 nm SiO_2 by spin coating a polymer solution (15 μL, 4 mg/mL in chloroform, 1000 rpm/30 s). The spin-coated film was annealed at 120 °C, 140 °C, 160 °C, and 175 °C for 30 min in golvebox. For the OTS modification, the silicon wafer was first cleaned with hot piranha solution (H_2SO_4 (98%): H_2O_2 (30% water solution) = 2:1). It was then further subjected to sonication sequentially in water and acetone for 5 min each. After drying at an oven, the silicon wafer was then put in a Petri dish with a small drop of OTS. The dish was then covered and heated in a vacuum oven at 120 °C for 3 h resulting in the formation of an OTS self-assembled monolayer on the surface. The OTS-modified substrates were rinsed successively with hexane, ethanol, and chloroform, and dried by nitrogen. Atomic force microscopy (AFM) (veeco dimension 3100) and GIXRD were used to characterize the film morphology. GIXRD measurements were performed at beamline 8-ID-E of Advanced Photon Source at the Argonne National Laboratory. Data were collected under helium environment with an incident beam energy at 10.82 keV and an incident angle at 0.14° on a two-dimensional detector (Pilatus 1M). GIXSGUI written for Matlab was used to apply corrections for detector nonuniformity, beam polarization, and detector sensitivity, and to reshape the 2-dimensional data into the representation q_z vs q_r (= $\sqrt{q_x^2 + q_y^2}$). The geometric corrected relative population by multiplying $\sin(\chi)$ with the extracted intensity of the (010) $\pi-\pi$ stacking peak $I(\chi)$ over the range of 88° < χ < 13° with 15 5° sector cut increment.

Device Fabrication and Measurement. The capacitance of OTS-modificated Si/SiO_2 substrates was 11 nF/cm^2, and was used for mobility calculation. The Si wafer was served as the gate electrode and SiO_2 as the dielectric. The gold souce/drain electrodes were sputtered and patterned by photolithography technique and OFETs were constructed in a bottom-contact, bottom-gate configuration. The device channel length investigated was 40 μm and the width was 1400 μm. Device characterization of the fabricated polymer OFETs was carried out using Keithley 4200 in ambient air. The field-effect mobility was calculated in the saturation regime by using the equation $I_{DS} = (\mu WC_i/2L)(V_G - V_T)^2$, where I_{DS} is the drain-source current, μ is the field-effect mobility, W is the channel width, L is the channel length, C_i is the capacitance per unit area of the gate dielectric layer, V_G is the gate voltage, and V_T is the threshold voltage.

Mechanical Properties Measurement by Buckling Method. Buckling method, proposed by Stafford et al.,[28] is the most accepted technique to measure the elastic modulus of the materials. The procedure starts by transferring a thin film of the material onto the prestrained polydimethylsiloxane (PDMS) substrate. Here PDMS was prepared by mixing the base and the curing agent at a ratio of 10:1 (by mass). After degassed in the vacuum, the PDMS was heated at the temperature of 60 °C for 2 h. The PDMS was cut into strips with the size of 1 cm × 7 cm × 2 mm. The modulus of PDMS was measured by stretching stage (ESM303, Mark-10) and force gauge (Series 5, Mark-10) by plotting the strain−stress curve. The modulus of the PDMS curing at the temperature of 60 °C for 2 h was ∼1 MPa; after annealing the PDMS at the temperature of 140 °C for 10 min, the modulus increased to ∼1.6 MPa. The cover glass (thickness ∼220 μm) was cut into the size of 1 × 1 cm^2. Before spin coating process (1500 rpm, 10 s), the glass wafers were treated with uv-ozone for 30 min. The wafers with the semiconducting polymer layer on top were placed face down on the prestrained (3% strain) PDMS, which were then immersed in water. As the wafer was hydrophilic and the PDMS was hydrophobic, water would move into the interface between the polymer and the glass wafer to separate them apart. As a result, the film would be transferred onto the PDMS. The whole transfer process took about 30 min. The transferred film was left in the air for 2 h for the evaporation of the water on the sample surface. After the strain applied on the PDMS was released, the buckles would form on the semiconducting polymer simultaneously. The modulus of the polymer film could be calculated from the eq 1:

$$E_f \approx 3E_s \times \left(\frac{1 - \nu_f^2}{1 - \nu_s^2}\right) \times \left(\frac{\lambda}{2\pi h}\right)^3 \quad (1)$$

where E is the modulus of the thin film materials, ν is the Poisson ratio, h is the thickness of the film, and λ is the period of the buckles. Subscripts s and f stand for substrate and film, respectively. The thicknesses were measured by AFM; and the period of the buckles could be obtained by using fast Fourier transform (FFT).

Mechanical Properties Measurement by Nanoindentation. Uniform and smooth films (thickness beyond several micrometers) of the three polymers were obtained using a hot-pressed annealing method.[29] Each polymer solid was sandwiched between two OTS-modified SiO_2/Si wafers on a hot plate. After being heated to 240 °C, the solid was pressed (∼10 kN cm^{-2}) by a heavy object. The polymer solid then became soft and film could be attained after 4 h heating. Nanoindention measurement[30,31] (G200, Keysight) with the Berkovich tip was used to achieve the mechnical properties of the thin films based on the three polymers. Twenty indentations were conducted on each sample. The tests were conducted in the glovebox with the temperature of 21 °C, the oxygen content is lower than 5 ppm, the water content is less than 10 ppm. The initial setup conditions of the

DOI: 10.1021/acsami.7b07624
ACS Appl. Mater. Interfaces 2017, 9, 25426−25433

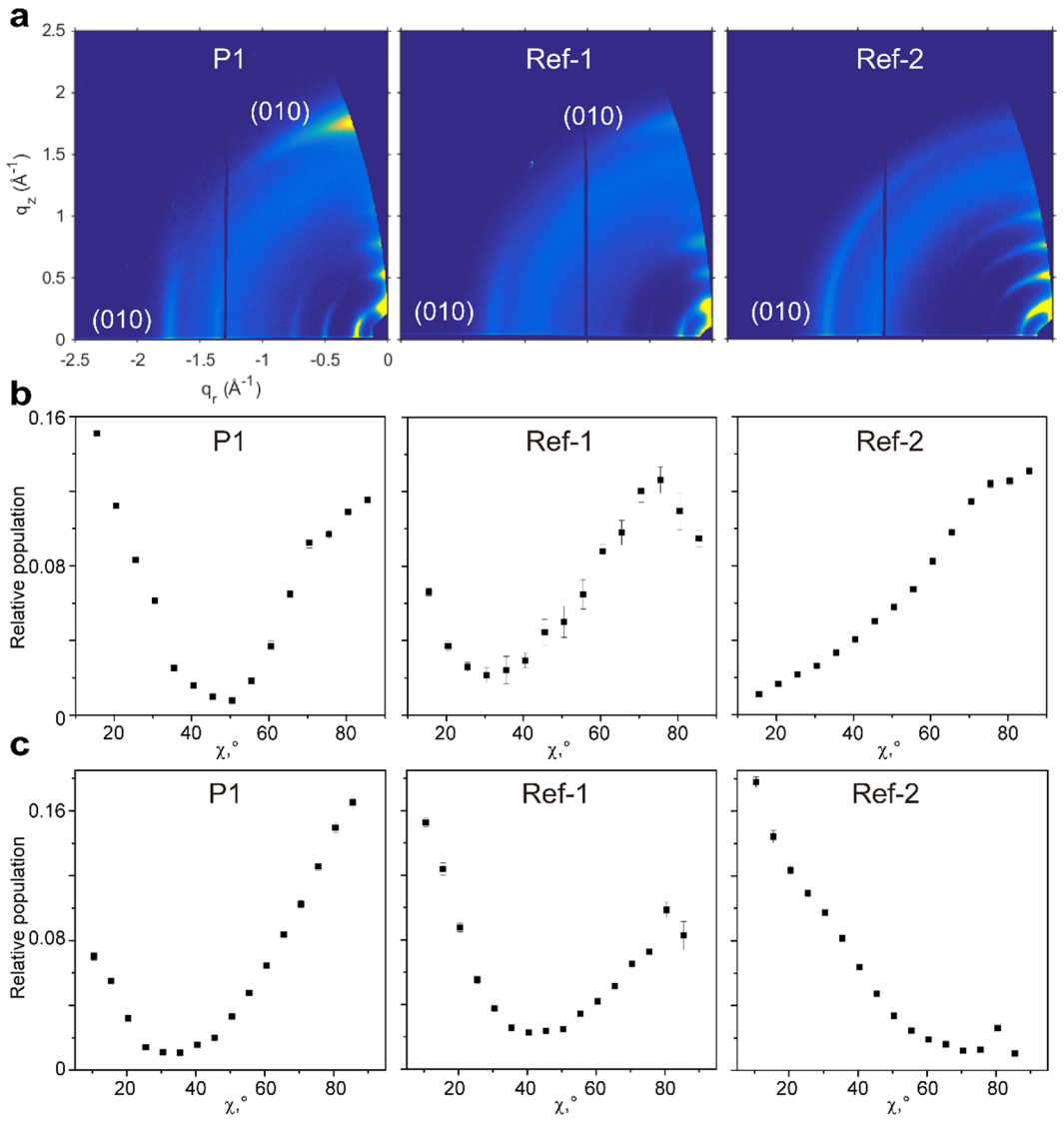

Figure 1. Polymer crystallite orientation and surface morphology of the three polymer thin films annealed at 160 °C. (a) GIXRD patterns of the annealed polymer films. (b, c) Comparison of the orientation distribution of the polymer films. (b) Pole figures of (010) and peaks for P1, Ref-1 and Ref-2. At $\chi = 0°$, the crystallites are face on; at $\chi = 90°$, the crystallites are edge on. (c) Pole figures of (100) peaks for P1, Ref-1 and Ref-2. $\chi = 0°$ represents edge on orientation, $\chi = 90°$ represents face-on orientation.

Berkovich tip were shown in Table S1 of the Supporting Information (SI).

RESULTS AND DISCUSSION

The synthetic route of the target polymer and the two reference polymers is shown in Scheme 1. The target monomer with asymmetric side chains was synthesized from 6,6′-dibromoisoindigo in two steps. In the first step, a 1:1 mixture of 11-(3-iodopropyl)henicosane and 6-iodohex-1-ene was reacted with 6,6′-isoindigo wih the presence of base under elevated temperature to form the intermediate with both 4-decyltetradecyl and hex-5-en-1-yl side chains, which could be easily separated from the symmetric analogues with silica gel chromatography. The intermediate was then reacted with 1,1,1,3,5,5,5-heptamethyltrisiloxane under the presence of Karstedt's catalyst to give the monomer with both branched-alkyl and siloxane-terminated side chains. The target and the reference polymers were synthesized by Stille polymerization and purified using Sohxlet extractions with acetone, hexanes and chloroform. The chloroform fractions were collected and palladium was further removed using *N*,*N*-diethylphenylazothioformamide.[15,27,32] P1 showed extremely good solubility in chloroform, dichlorobenzene and trichlorobenzene, and also in nonchlorinated solvents, such as *m*-xylene and tetrahydrofuran.

The physical properties of the three polymers are summarized in Table S2. The molecular weights of the polymers were measured using GPC with trichlorobenzene at 150 °C. The number-averaged molecular weight (M_n) of P1 is 35.6 kDa with a polydispersity index (PDI) of 5.1. The bimodal feature of the peak suggests aggregation of the polymer molecules in the solution even at 150 °C. As a comparison, the M_n of Ref-2 was measured to be 28.8 kDa with PDI of 4.0, which was comparable with previous result from literature (39.2 kDa, PDI = 3.2)[26] and P1. On the contrary, the M_n obtained for Ref-1 (8.5 kDa, PDI = 1.9) was significantly smaller compared to the other polymers, which could be attributed to the lower solubility of Ref-1, which led to the loss of high molecular weight fractions in the sample preparation for the GPC analysis. The absorption spectra of the three polymers in chloroform

DOI: 10.1021/acsami.7b07624
ACS Appl. Mater. Interfaces 2017, 9, 25426−25433

Table 1. Relevant Crystallographic Parameters for the Three Polymer Films

polymers	$\pi-\pi$ spacing (Å)	in-plane fwhm	lamellar spacing (Å)	Out-of-plane fwhm
P1	3.58	0.085	23.7	0.053
Ref-1	3.56 [3.58]	0.127	23.3 [22.8]	0.047
Ref-2	3.59 [3.57]	0.168	24.4 [24.7]	0.046

[a]Data shown in brackets are adapted from refs 15 and 26.

Table 2. OFET Properties of the Three Polymers

polymers	as-spun	annealed at 160 °C		
	average μ ($cm^2\ V^{-1}\ s^{-1}$)	average μ [highest μ] ($cm^2\ V^{-1}\ s^{-1}$)	I_{on}/I_{off}	V_T (V)
P1	0.91	3.8 ± 0.7 [5.1]	$>10^5$	−2
Ref-1	0.13	0.47 ± 0.04 [0.52]	$>10^3$	0.7
Ref-1[a]	0.45	2.00 ± 0.49 [2.48]	$>10^5$	3
Ref-2	0.12	0.51 ± 0.18 [0.77]	$>10^4$	−2
Ref-2[b]	NA	2.98 [3.62]	$>10^6$	−5

[a]Data from ref 15. [b]Data from ref 26.

solution and as thin film are shown in Figure S5. In chloroform solutions, all polymers exhibit dual-band absorbance spectra with the highest peaks appearing around 720 nm and a shoulder around 660 nm. For P1 and Ref-1, the shoulders of the thin film shift to shorter wavelengths by about 20 nm, while the highest peaks remain almost unchanged. It was also noted that, in comparison with P1 and Ref-2, Ref-1 has limited solubility in most organic solvents under ambient conditions, including chloroform and chlorobenzene. The optical images of polymer solutions and thin films are displayed in Figures S6 and S7. Particles and aggregates are visible in Ref-1 chloroform solution and thin film. The thermal stability of P1 is confirmed by TGA. No noticeable decomposition is observed until around 390 °C (Figure S8), which is comparable with the reference polymers. Phase transition properties are evaluated using DSC and no phase transition could be observed in the range of 0−300 °C (Figure S9).

To probe the impact of the asymmetric side chains on thin film morphology and molecular packing, GIXRD measurement was first carried out. P1 thin film was obtained via spin-coating from its chloroform (4 mg/mL) solution on top of the OTS-modified SiO_2/Si substrate. The reference polymer thin films were prepared by following the same protocol. These thin films were then annealed at 160 °C before the morphology examination. Figure 1a shows the 2D GIXRD patterns of the three polymers, and the crystallographic parameters are summarized in Table 1. The $\pi-\pi$ stacking distances of 3.58 Å, 3.56 Å, 3.59 Å and lamellar packing distances of 23.7 Å, 23.3 Å, 24.4 Å were observed for P1, Ref-1 and Ref-2, respectively. The data of Ref-1 and Ref-2 are in good agreement with the reported values in the literature.[15,26] The GIXRD pattern of Ref-2 illustrates a long-range ordered edge-on lamellar packing, corresponding with the literature report.[26] Ref 1 shows a weak bimodal feature, the same as Bao et al. reported.[15] From the GIXRD pattern of P1, a much more distinct bimodal packing with both the edge on (χ = 90°) and the face on (χ = 0°) orientations of $\pi-\pi$ stacking can be observed. The lamellar stacking peaks (h00) near χ = 0° and χ = 90° on the GIXRD pattern also indicate bimodal distribution. Meanwhile, compared with Ref-1, P1 shows clear long-range ordered lamellar packing (h00) along both directions. The pattern for Ref-1 shows much weaker face on (010) peak compared to P1, indicating a weak bimodal distribution with mainly edge-on crystallites. The pattern for Ref-2 with dominant edge-on (010) peak at χ = 90° and edge-on (h00) peaks at χ = 0° indicates strongly preferred edge-on stacking. To quantitatively compare the orientation distributions, we analyzed the geometric-corrected relative population of crystallites of various orientations, $I(\chi)\sin(\chi)$, from the (010) $\pi-\pi$ stacking peak. $I(\chi)\sin(\chi)$ is the geometrically corrected diffraction intensity that scales with percentage of crystallites oriented χ degrees from the substrate normal, thereby representing the relative population of these crystallites. The out-of-plane orientation distribution is represented by the polar angle χ. For instances, for the (010) peak, face-on crystallites correspond to χ = 0° and edge-on crystallites to χ = 90°. We have also performed pole figure analysis for the (100) peaks for P1, Ref-1 and Ref-2 and compared the (100) pole figures with the previously included (010) pole figures. For (100) analysis, χ = 90° represents face-on orientation, whereas for (010) analysis, χ = 0° represents face-on orientation. Judged from (100) peak analysis, population of crystallizes with face-on orientation substantially increases in the order Ref-2 < Ref-1 < P1, which is consistent with the result of (010) analysis. The bimodal orientation distribution for P1 is demonstrated in the pole figures from both (010) and (100) peaks. For P1, the higher population at low χ angles in the (010) pole figure indicates moderately preferred face-on orientation, agreeing with the higher population at high χ angles in the (100) pole figure. Ref-1 shows weak bimodal distribution with preferred edge-on orientation and Ref-2 shows predominately edge-on orientation, illustrated by the high population at high χ angles in the (010) pole figures and the high population at low χ angles in the (100) pole figures. The specific percentages of orientation distributions are displayed in Table S3. From the pole figure analysis for the (100) and (010) peaks, thus, we can conclude that the bimodal packing in P1 thin film is an evident proof for the success of our molecular design. By introducing the asymmetric side chains, the population of face-on crystallites substantially increased compared to the references, and bimodal distribution of crystallite orientation has been achieved. One possible explanation for change of packing modes from the edge-on dominant fashion to the bimodal orientation is that the design of asymmetric side chains introduces a new interaction between different side chains that induces the change of packing habit. We then applied tapping-mode AFM to examining the surfaces of the films (Figure S10). The AFM image of P1 thin film shows scaled crystalline structures with

DOI: 10.1021/acsami.7b07624
ACS Appl. Mater. Interfaces 2017, 9, 25426−25433

interconnected-networks. Compared to the morphologies of Ref-1 and Ref-2, P1 thin film appears to have large crystalline aggregates. This observation is in a good agreement with a smaller in-plane full-width half-maximum (fwhm) obtained in GIXRD measurements shown in Table 1.

OFETs were fabricated to evaluate charge transport properties of three polymers on prepatterned source-drain contacts on a silicon wafer with a bottom-gate/bottom-contact configuration. The width of the channel is 1400 μm, and the length is 40 μm. Thin films were obtained with the same method used for GIXRD and AFM measurements. The FET characteristics of P1 were investigated in ambient air on 20 different devices that were previously annealed at various temperatures inside a N_2 glovebox. The saturation regime mobility was then calculated and summarized along with relevant OFET parameters. The devices without annealing showed an average mobility of 0.91 $cm^2\ V^{-1}\ s^{-1}$. After annealing, the mobility values increased largely. The devices annealed at 160 °C offered the best performance (Figure S11) and an average mobility of 3.8 ± 0.7 $cm^2\ V^{-1}\ s^{-1}$ was achieved (Table 2, Figure S12a). Typical transfers and output characteristics of OFET are displayed in Figures 2 and S13, with

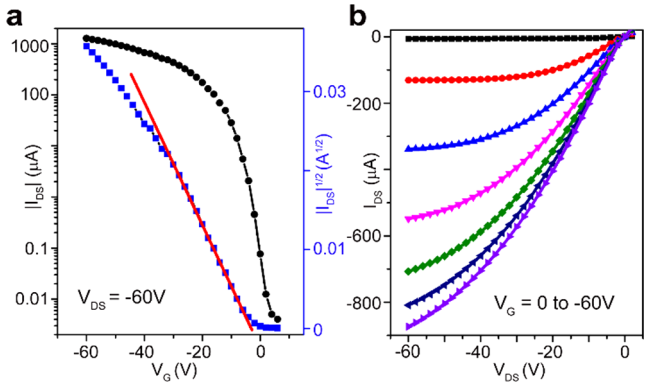

Figure 2. Typical transfer (a) and output (b) characteristics of FET based on P1.

excellent gate modulation, and almost no hysteresis was observed (Figure S13). The exhibited transfer curve, however, exists a bit of deviation from an ideal transfer curve, as we could find a small kink behavior at the end of the $(I_{DS})^{1/2}$ versus V_G curve.[33] Several suggestions have been made to explain the nonideal transfer curves, such as contact resistance effect or the nonsaturated behavior in high V_G region.[2,34,35] The electron trapping of the SiO_2 dielectric layer used in our transistors might be another factor.[36] Nevertheless, here the gate voltage regions where we extracted mobility are not narrow, nor low of only a few volts in the subthreshold regime, thus the equation $(I_{DS} = (\mu WC_i/2L)(V_G - V_T)^2)$ is still applicable. In addition, an on-to-off current ratio (I_{on}/I_{off}) > 10^5 and average threshold voltage (V_T) of −2.0 V were also obtained (Table 2). The maximum mobility of devices reached 5.1 $cm^2\ V^{-1}\ s^{-1}$, higher than the two reference polymers reported in the literatures (2.48 $cm^2\ V^{-1}\ s^{-1}$ for Ref-1 and 3.62 $cm^2\ V^{-1}\ s^{-1}$ for Ref-2, Table 2). Furthermore, the devices exhibited good stability against atmospheric oxygen, with only slight degradation in mobility when the films were stored under ambient conditions (the polymer maintained more than 60% of the initial mobility value in more than one month, RH = 45−50%) (Figure S12b).

As a further comparison, we also investigated the OFETs characteristic of Ref-1 and Ref-2. As shown in Table 2, the mobility values of Ref-1 and Ref-2 were similar, but lower than the reported values. Typical transfers and output characteristics of OFETs based on Ref-1 and Ref-2 are displayed in Figures S13 and S14. The discrepancy is likely caused by different processing methods applied here and in literature, as well as the different device configurations for OFETs. The poor solubility of ref-1 also prevented a further optimization. We could also observe a bit hysteresis of ref-1 (Figure S13), mainly due to the interface morphology resulting from the poor solubility. Nevertheless, P1 evidently outperforms ref-1 and ref-2. The larger crystalline aggregates of P1 observed from the AFM image and in-plane fwhm is one of the factors contributing to the high mobility. But more crucially, considering similarity in their electronic structures, we believe the efficient charge transport behaviors in P1 thin films are ascribed to the formation of a bimodal orientation with both edge-on and face-on packing motifs, namely a more effective 3D conduction network. With the proposed 3D conduction channel for charge transport in semiconducting polymer thin films, charge carriers transport primarily along the in-plane direction, and are able to change to out-of-plane direction when encountering the gain boundaries, ultimately harvesting higher charge mobility.[22,23]

With elucidating the impact of asymmetric side chains on polymer packing and charge transport properties, we further studied their effect on the mechanical properties. Mechanical properties of semiconducting polymers have received much less attention in comparison with their optical and electronic properties. The relationship between mechanical properties and molecular structures is still largely unexplored for semiconducting polymers until recently.[37,38] The ability to tune mechanical properties is highly desired for semiconducting polymers, because they play an important role in the durability and conformability of the corresponding electronic devices. Buckling method and nanoindention measurement were both performed on P1, Ref-1 and Ref-2. The results of the three samples from buckling method are 0.151 GPa, 0.338 GPa, and 0.242 GPa for P1, Ref-1 and Ref-2, respectively, and using nanoindentation measurement, P1 exhibited tensile modulus values of 0.179 ± 0.022 GPa, while Ref-1 and Ref-2 showed 0.342 ± 0.012 GPa and 0.282 ± 0.022 GPa, respectively, as summarized in Figure 3. The data for the three polymers using the two methods are consistent and both of the results illustrate that P1 shows the lowest modulus values. These numbers are in the low end of reported values in literature, 0.22 to 1.33 GPa.[39,40] In the thin film of P1, the combination of edge on orientation and face-on orientation make it possible that the overlapping region of the two directions might be softer than the other area, and as a consequence, less degree of interchain π-stacking in the crystalline regions of the film and fewer van-der-Waals bonds needed to be conquered. Thus, the bimodal orientation modifies the mechanical property. Ref-1, however, exhibited poor solubility, mainly resulting from the strong interchain interactions, which led to the highest modulus values.[41]

CONCLUSIONS

We have successfully synthesized P1 with asymmetric side chains and showed that breaking symmetry in side chains is an efficient method to alter the arrangement of molecular orientations. The bimodal orientation observed in P1 enhances 3D charge transport and the average mobility obtained reaches

DOI: 10.1021/acsami.7b07624
ACS Appl. Mater. Interfaces 2017, 9, 25426−25433

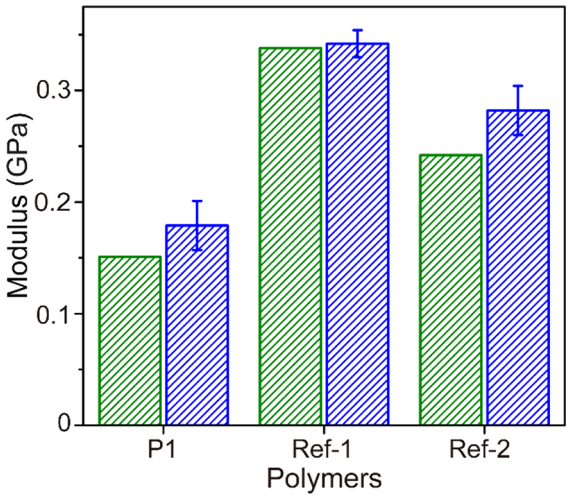

Figure 3. Mechanical properties of the three polymers. The data of olive histogram are from buckling method and the data of the blue histogram are from nanoindentation measurement.

3.8 ± 0.7 $cm^2 V^{-1} s^{-1}$, with the highest mobility of 5.1 $cm^2 V^{-1} s^{-1}$. P1 also exhibits excellent solubility in a wide range of organic solvents because of the asymmetric side chains. The nanoindentation measurement reveals that breaking symmetry in side chains also has an impact on the mechanical properties of the polymer, providing a lower tensile modulus both from bucking method (0.151 GPa) and nanoindentation measurement (0.179 ± 0.022 GPa). These observations bode well for the concept of symmetry breaking side chains in developing high-performance semiconducting polymers.

■ ASSOCIATED CONTENT

Supporting Information

The Supporting Information is available free of charge on the ACS Publications website at DOI: 10.1021/acsami.7b07624.

Physical properties of P1, Ref-1 and Ref-2; NMR spectra of monomers and polymers; GPC traces of P1, Ref-1, and Ref-2; solution and thin film absorption spectra of P1, Ref-1, and Ref-2; optical images of P1, Ref-1, and Ref-2; TGA and DSC thermal histogram of P1; AFM images of P1, Ref-1, and Ref-2; and FET characteristics of P1, Ref-1, and Ref-2 (PDF)

■ AUTHOR INFORMATION

Corresponding Authors

*E-mail: hanying_li@zju.edu.cn (H.L.).
*E-mail: jgmei@purdue.edu (J.M.).

ORCID

Ying Diao: 0000-0002-8984-0051
Jianguo Mei: 0000-0002-5743-2715

Author Contributions

▽These authors contributed equally to this work.

Notes

The authors declare no competing financial interest.

■ ACKNOWLEDGMENTS

The work was supported by the startup fund from Purdue University, the Office of Naval Research Young Investigator Program (ONR YIP), award number N00014-16-1-2551, and MOE Key Laboratory of Macromolecular Synthesis and Functionalization, Zhejiang University (2016MSF003). G.X. acknowledges the financial support from the China Scholar Council. This research used resources of the Advanced Photon Source, a U.S. Department of Energy (DOE) Office of Science User Facility operated for the DOE Office of Science by Argonne National Laboratory under Contract No. DE-AC02-06CH11357.

■ REFERENCES

(1) Mei, J. G.; Diao, Y.; Appleton, A. L.; Fang, L.; Bao, Z. N. Integrated Materials Design of Organic Semiconductors for Field-Effect Transistors. *J. Am. Chem. Soc.* **2013**, *135*, 6724−6746.
(2) Sirringhaus, H. 25th Anniversary Article: Organic Field-Effect Transistors: the Path Beyond Amorphous Silicon. *Adv. Mater.* **2014**, *26*, 1319−1335.
(3) Lu, L. Y.; Zheng, T. Y.; Wu, Q. H.; Schneider, A. M.; Zhao, D. L.; Yu, L. P. Recent Advances in Bulk Heterojunction Polymer Solar Cells. *Chem. Rev.* **2015**, *115*, 12666−12731.
(4) Grimsdale, A. C.; Chan, K. L.; Martin, R. E.; Jokisz, P. G.; Holmes, A. B. Synthesis of Light-Emitting Conjugated Polymers for Applications in Electroluminescent Devices. *Chem. Rev.* **2009**, *109*, 897−1091.
(5) Zhao, Y.; Guo, Y. L.; Liu, Y. Q. 25th Anniversary Article: Recent Advances in n-Type and Ambipolar Organic Field-Effect Transistors. *Adv. Mater.* **2013**, *25*, 5372−5391.
(6) Horowitz, G. Organic Field-Effect Transistors. *Adv. Mater.* **1998**, *10*, 365−377.
(7) Horowitz, G. Organic Thin Film Transistors: From Theory to Real Devices. *J. Mater. Res.* **2004**, *19*, 1946−1962.
(8) Street, R. A.; Northrup, J. E.; Salleo, A. Transport in Polycrystalline Polymer Thin-Film Transistors. *Phys. Rev. B: Condens. Matter Mater. Phys.* **2005**, *71*, 165205.
(9) Salleo, A. Charge Transport in Polymeric Transistors. *Mater. Today* **2007**, *10*, 38−45.
(10) Sirringhaus, H.; Brown, P. J.; Friend, R. H.; Nielsen, M. M.; Bechgaard, K.; Langeveld-Voss, B. M. W.; Spiering, A. J. H.; Janssen, R. A. J.; Meijer, E. W.; Herwig, P.; de Leeuw, D. M. Two-Dimensional Charge Transport in Self-Organized, High-Mobility Conjugated Polymers. *Nature* **1999**, *401*, 685−688.
(11) Coropceanu, V.; Cornil, J.; da Silva, D. A.; Olivier, Y.; Silbey, R.; Bredas, J. L. Charge Transport in Organic Semiconductors. *Chem. Rev.* **2007**, *107*, 2165−2165.
(12) Chabinyc, M. L.; Toney, M. F.; Kline, R. J.; McCulloch, I.; Heeney, M. X-ray Scattering Study of Thin Films of Poly(2,5-bis(3-alkylthiophen-2-yl)thieno[3,2-b]thiophene. *J. Am. Chem. Soc.* **2007**, *129*, 3226−3237.
(13) Schuettfort, T.; Thomsen, L.; McNeill, C. R. Observation of a Distinct Surface Molecular Orientation in Films of a High Mobility Conjugated Polymer. *J. Am. Chem. Soc.* **2013**, *135*, 1092−1101.
(14) Kronemeijer, A. J.; Pecunia, V.; Venkateshvaran, D.; Nikolka, M.; Sadhanala, A.; Moriarty, J.; Szumilo, M.; Sirringhaus, H. Two-Dimensional Carrier Distribution in Top-Gate Polymer Field-Effect Transistors: Correlation between Width of Density of Localized States and Urbach Energy. *Adv. Mater.* **2014**, *26*, 728−733.
(15) Mei, J. G.; Kim, D. H.; Ayzner, A. L.; Toney, M. F.; Bao, Z. N. Siloxane-Terminated Solubilizing Side Chains: Bringing Conjugated Polymer Backbones Closer and Boosting Hole Mobilities in Thin-Film Transistors. *J. Am. Chem. Soc.* **2011**, *133*, 20130−20133.
(16) Lee, J.; Han, A. R.; Yu, H.; Shin, T. J.; Yang, C.; Oh, J. H. Boosting the Ambipolar Performance of Solution-Processable Polymer Semiconductors via Hybrid Side-Chain Engineering. *J. Am. Chem. Soc.* **2013**, *135*, 9540−9547.
(17) Kim, Y.; Long, D. X.; Lee, J.; Kim, G.; Shin, T. J.; Nam, K. W.; Noh, Y. Y.; Yang, C. A Balanced Face-On to Edge-On Texture Ratio in Naphthalene Diimide-Based Polymers with Hybrid Siloxane Chains Directs Highly Efficient Electron Transport. *Macromolecules* **2015**, *48*, 5179−5187.

DOI: 10.1021/acsami.7b07624
ACS Appl. Mater. Interfaces 2017, 9, 25426−25433

(18) Zhang, X. R.; Richter, L. J.; DeLongchamp, D. M.; Kline, R. J.; Hammond, M. R.; McCulloch, I.; Heeney, M.; Ashraf, R. S.; Smith, J. N.; Anthopoulos, T. D.; Schroeder, B.; Geerts, Y. H.; Fischer, D. A.; Toney, M. F. Molecular Packing of High-Mobility Diketo Pyrrolo-Pyrrole Polymer Semiconductors with Branched Alkyl Side Chains. *J. Am. Chem. Soc.* **2011**, *133*, 15073−15084.
(19) Ayzner, A. L.; Mei, J. G.; Appleton, A.; DeLongchamp, D.; Nardes, A.; Benight, S.; Kopidakis, N.; Toney, M. F.; Bao, Z. N. Impact of the Crystallite Orientation Distribution on Exciton Transport in Donor-Acceptor Conjugated Polymers. *ACS Appl. Mater. Interfaces* **2015**, *7*, 28035−28041.
(20) Han, A. R.; Lee, J.; Lee, H. R.; Lee, J.; Kang, S. H.; Ahn, H.; Shin, T. J.; Oh, J. H.; Yang, C. Siloxane Side Chains: A Universal Tool for Practical Applications of Organic Field-Effect Transistors. *Macromolecules* **2016**, *49*, 3739−3748.
(21) Demeyu, L.; Stafstrom, S.; Bekele, M. Monte Carlo Simulations of Charge Carrier Mobility in Semiconducting Polymer Field-Effect Transistors. *Phys. Rev. B: Condens. Matter Mater. Phys.* **2007**, *76*, 155202.
(22) Sharma, A.; van Oost, F. W. A.; Kemerink, M.; Bobbert, P. A. Dimensionality of Charge Transport in Organic Field-Effect Transistors. *Phys. Rev. B: Condens. Matter Mater. Phys.* **2012**, *85*, 235302.
(23) Park, S.; Lee, M. H.; Ahn, K. S.; Choi, H. H.; Shin, J.; Xu, J.; Mei, J.; Cho, K.; Bao, Z.; Lee, D. R.; Kang, M. S.; Kim, D. H. Combinatorial Study of Temperature-Dependent Nanostructure and Electrical Conduction of Polymer Semiconductors: Even Bimodal Orientation Can Enhance 3D Charge Transport. *Adv. Funct. Mater.* **2016**, *26*, 4627−4634.
(24) Shehu, A.; Quiroga, S. D.; D'Angelo, P.; Albonetti, C.; Borgatti, F.; Murgia, M.; Scorzoni, A.; Stoliar, P.; Biscarini, F. Layered Distribution of Charge Carriers in Organic Thin Film Transistors. *Phys. Rev. Lett.* **2010**, *104*, 246602.
(25) Mei, J. G.; Bao, Z. N. Side Chain Engineering in Solution-Processable Conjugated Polymers. *Chem. Mater.* **2014**, *26*, 604−615.
(26) Lei, T.; Dou, J. H.; Pei, J. Influence of Alkyl Chain Branching Positions on the Hole Mobilities of Polymer Thin-Film Transistors. *Adv. Mater.* **2012**, *24*, 6457−6461.
(27) Mei, J.; Graham, K. R.; Stalder, R.; Reynolds, J. R. Synthesis of Isoindigo-based Oligothiophenes for Molecular Bulk Heterojunction Solar Cells. *Org. Lett.* **2010**, *12*, 660−663.
(28) Stafford, C. M.; Harrison, C.; Beers, K. L.; Karim, A.; Amis, E. J.; Vanlandingham, M. R.; Kim, H. C.; Volksen, W.; Miller, R. D.; Simonyi, E. E. A Buckling-based Metrology for Measuring the Elastic Moduli of Polymeric Thin Films. *Nat. Mater.* **2004**, *3*, 545−550.
(29) Zhao, Y.; Zhao, X.; Roders, M.; Gumyusenge, A.; Ayzner, A. L.; Mei, J. Melt-Processing of Complementary Semiconducting Polymer Blends for High Performance Organic Transistors. *Adv. Mater.* **2017**, *29*, 1605056.
(30) Oliver, W. C.; Pharr, G. M. An Improved Technique for Determining Hardness and Elastic-Modulus Using Load and Displacement Sensing Indentation Experiments. *J. Mater. Res.* **1992**, *7*, 1564−1583.
(31) VanLandingham, M. R.; Villarrubia, J. S.; Guthrie, W. F.; Meyers, G. F. Nanoindentation of Polymers: an Overview. *Macromol. Symp.* **2001**, *167*, 15−43.
(32) Nielsen, K. T.; Bechgaard, K.; Krebs, F. C. Removal of Palladium Nanoparticles from Polymer Materials. *Macromolecules* **2005**, *38*, 658−659.
(33) McCulloch, I.; Salleo, A.; Chabinyc, M. Avoid the Kinks When Measuring Mobility Transistor Measurements Can Overstate Organic Semiconductor Charge Carrier Mobility. *Science* **2016**, *352*, 1521−1522.
(34) Zheng, Y. Q.; Lei, T.; Dou, J. H.; Xia, X.; Wang, J. Y.; Liu, C. J.; Pei, J. Strong Electron-Deficient Polymers Lead to High Electron Mobility in Air and Their Morphology-Dependent Transport Behaviors. *Adv. Mater.* **2016**, *28*, 7213−7219.
(35) Bittle, E. G.; Basham, J. I.; Jackson, T. N.; Jurchescu, O. D.; Gundlach, D. J. Mobility Overestimation due to Gated Contacts in Organic Field-Effect Transistors. *Nat. Commun.* **2016**, *7*, 10908.
(36) Phan, H.; Wang, M.; Bazan, G. C.; Nguyen, T. Q. Electrical Instability Induced by Electron Trapping in Low-Bandgap Donor-Acceptor Polymer Field-Effect Transistors. *Adv. Mater.* **2015**, *27*, 7004−7009.
(37) Savagatrup, S.; Printz, A. D.; O'Connor, T. F.; Zaretski, A. V.; Rodriquez, D.; Sawyer, E. J.; Rajan, K. M.; Acosta, R. I.; Root, S. E.; Lipomi, D. J. Mechanical Degradation and Stability of Organic Solar Cells: Molecular and Microstructural Determinants. *Energy Environ. Sci.* **2015**, *8*, 55−80.
(38) Savagatrup, S.; Zhao, X. K.; Chan, E.; Mei, J. G.; Lipomi, D. J. Effect of Broken Conjugation on the Stretchability of Semiconducting Polymers. *Macromol. Rapid Commun.* **2016**, *37*, 1623−1628.
(39) Rodriquez, D.; Kim, J. H.; Root, S. E.; Fei, Z. P.; Boufflet, P.; Heeney, M.; Kim, T. S.; Lipomi, D. J. Comparison of Methods for Determining the Mechanical Properties of Semiconducting Polymer Films for Stretchable Electronics. *ACS Appl. Mater. Interfaces* **2017**, *9*, 8855−8862.
(40) Wu, H. C.; Hung, C. C.; Hong, C. W.; Sun, H. S.; Wang, J. T.; Yamashita, G.; Higashihara, T.; Chen, W. C. Isoindigo-Based Semiconducting Polymers Using Carbosilane Side Chains for High Performance Stretchable Field-Effect Transistors. *Macromolecules* **2016**, *49*, 8540−8548.
(41) Wang, G. J. N.; Shaw, L.; Xu, J.; Kurosawa, T.; Schroeder, B. C.; Oh, J. Y.; Benight, S. J.; Bao, Z. N. Inducing Elasticity through Oligo-Siloxane Crosslinks for Intrinsically Stretchable Semiconducting Polymers. *Adv. Funct. Mater.* **2016**, *26*, 7254−7262.

DOI: 10.1021/acsami.7b07624
ACS Appl. Mater. Interfaces 2017, 9, 25426−25433